24th COBEM - 2017

24th ABCM International Congress of Mechanical Engineering
December 3-8, 2017, Curitiba, PR, Brazil

COBEM-2017-0427
NUMERICAL SIMULATION OF GAS AND LIQUID IN INTERNAL LOOP AIRLIFT REACTOR

Roberto Francisco da Silva
Viviana Cocco Mariani
Pontifical Catholic University of Parana. R. Imac. Conceição, 1155 - Prado Velho, Curitiba - PR, Brazil
roberto.302v8@gmail.com, viviana.mariani@pucpr.br

Abstract. *The main idea of this study is verifying previously data in CFD simulations of hydrodynamics in an internal-loop airlift reactor. The CFD simulations were done in commercial code CFX 17.2 using the Euler-Euler model for multiphase flow and boundaries conditions in accordance with the literature. Gas superficial velocities in riser were in range from 0.01 to 0.075 m/s. The simulation was done to study the global flow characteristics as air holdup and liquid interstitial velocity in the riser and downcomer. The results are in agreement with those obtained in literature except at the highest surface velocity of the gas where all results are underestimated.*

Keywords: *Airlift. CFD, Multiphase flow, Simulation, Euler-Euler model.*

1. INTRODUCTION

The interest in reactors with pneumatic agitation for fermentative purposes has been increasing since 1969, mainly due to the low cost of manufacturing, low energy consumption and greater efficiency in the mass transport and energy phenomena (Chen, 1990).

Pneumatic reactors can be classified into bubble columns and airlifts. The main difference between them lies in the type of fluid flow, which depends on their geometry. The bubble column reactors are simple vessels with air injection, usually at the bottom, and produce a random movement due to the upward movement of the bubbles. In airlifts, the flow pattern depends on its geometry which has a channel for gas (liquid up flow) the riser and a separate channel for the downflow named downcomer. These two channels are attached at the top and bottom to form a closed loop. The gas is injected near the bottom of the riser and running through it, promoting the movement of the liquid and separating on the surface of the liquid in the section called the gas separator. However, a portion of the dispersed phase can be entrapped by the descending liquid to the downcomer, its depending on the geometry of the gas separator and the operating conditions, and it has a significant influence on the fluid dynamics in the reactor (Merchuk, 2002).

Even with the development and accelerated use of airlifts there are still difficulties in maintaining the stability and rates of the bioprocesses, resulting from the design and construction of the inadequate equipment, resulting in an inappropriate mixture and consequently putting at risk the whole fermentative process. A good blend is necessary to avoid thermal stratification, homogenize the pH, promote the interaction between microorganism and substrate and to promote the necessary gas exchanges (Mashhadani *et al*., 2015).

As the main use of the reactors were in fermentations, the initial studies in these equipments were focused on the rate of mass transfer between gas and liquid, more specifically of the oxygenation of the liquid, and in the efficiency of the agitation. Thus, the parameters that actually influenced the efficiency of the airlifts were the velocity profile and the gas holdup in the channels. The researchers looked for empirical relations of the parameters with the geometry of the equipment (Bello; Robinson; Moo-Young, 1985; Chisti, 1989; Merchuk *et al*., 1994; Siegel; Merchuck, 1988). In this way, the same parameters are studied until now, since they are the way to verify the performance of a geometry.

This work aims to verify the hydrodynamic results presented by Šimčík *et al*. (2011), which were later used by Xu *et al.* (2015) in order to improve the results of the gas holdup in the downcomer at high superficial velocities of air. With these results verified, new studies on other fronts could be conducted, improving the projects of these important equipment.

2. SIMULATION PROCEDURE

The computational simulations were done in commercial code CFX 17.2. The computational domain used is presented in Fig. 1 and follows the same dimensions used by Šimčík *et al*. (2011) and later by Xu *et al*. (2015), such dimensions are described in Table 1.

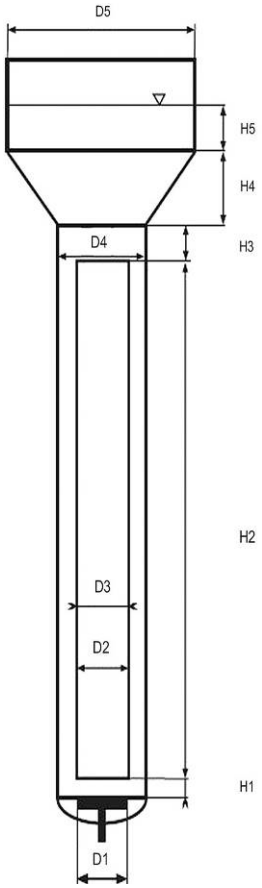

Figure 11. Airlift geometry (Šimčík *et al*. 2011)

Table 1. Airlift dimensions (see Fig. 1).

	(mm)
D1	100
D2	62
D3	70
D4	142
D5	420
H1	23
H2	1200
H3	200
H4	170
H5	120

The full Euler-Euler two-fluid model is used, the continuity and momentum equations are solved individually for each phase. The momentum equations are coupled together by pressure and interphase force terms. The points were setting according to the reading bulbs in the original experiment. Model equations and boundary conditions are described to follow.

Continuity equations are:

$$\frac{\partial \alpha_c \rho_c}{\partial t} + \nabla.(\partial \alpha_c \rho_c \mathbf{v}_c) = 0 \tag{1}$$

$$\frac{\partial \alpha_d \rho_d}{\partial t} + \nabla.(\partial \alpha_d \rho_d \mathbf{v}_d) = 0 \tag{2}$$

where α is the volumetric fraction of phase, ρ is the fluid density and *v* is the mean velocity of phase, the subscripts *c* and *d* are, respectively, the continuous and dispersed phases.

The momentum equations are:

$$\frac{\partial \alpha_c \rho_c \mathbf{v}_c}{\partial t} + \nabla.(\alpha_c \rho_c \mathbf{v}_c \mathbf{v}_c) = -\alpha_c \nabla p + \nabla.[\alpha_c \mu_{c,eff}(\nabla \mathbf{v}_c + \nabla \mathbf{v}_c^T) + \alpha_c \rho_c g + M_{cd} \tag{3}$$

$$\frac{\partial \alpha_d \rho_d \mathbf{v}_d}{\partial t} + \nabla.(\alpha_d \rho_d \mathbf{v}_d \mathbf{v}_d) = -\alpha_d \nabla p + \nabla.[\alpha_d \mu_{d,eff}(\nabla \mathbf{v}_d + \nabla \mathbf{v}_d^T) + \alpha_d \rho_d g + M_{dc} \tag{4}$$

where *p* is the pressure, *g* is the acceleration due to gravity, $M_{cd} = -M_{dc}$ is a force acting on the phase *c* due to phase *d*, and $\mu_{c,eff}$ and $\mu_{d,eff}$ are effective viscosities, $\mu_{c,eff} = \mu_c + \mu_{tc}$ and $\mu_{d,eff} = \mu_d + \mu_{td}$.

Drag force equation:

$$M_{cd,D} = K_{cd}(\mathbf{v}_d - \mathbf{v}_c) = \frac{3}{4}\left(\frac{C_D}{d}\right)\alpha_d \rho_c |\mathbf{v}_d - \mathbf{v}_c|(\mathbf{v}_d - \mathbf{v}_c) \quad (5)$$

here K means the momentum transfer coefficient, d means the bubble equivalent diameter, the drag coefficient was set to $C_D = 1.215$ as set by Šimčík *et al*. (2011).

Turbulence dispersion force equation:

$$M_{cd,TD} = C_{TD} K_{cd} \nu_{tc} / \sigma_{tc} \left(\frac{\nabla \alpha_d}{\alpha_d} - \frac{\nabla \alpha_c}{\alpha_c}\right) \quad (6)$$

where $C_{TD} = 1$, ν_{tc} is turbulent kinematic viscosity of the continuous phase and $\sigma_{tc} = 0.9$.

The k-ε model was used to model turbulence and to obtain a closure for turbulent viscosity in the continuous phase μ_{tc}:

$$\mu_{tc} = C_\mu \rho_c \left(\frac{k_c^2}{\varepsilon_c}\right) \quad (7)$$

$$\frac{\partial(\alpha_c \rho_c k_c)}{\partial t} + \nabla.(\alpha_c \rho_c \mathbf{v}_c k_c) = \nabla\left[\alpha_c\left(\mu_c + \frac{\mu_{tc}}{\sigma_k}\right)(\nabla k_c)\right] + \alpha_c G_c - \alpha_c \rho_c \varepsilon_c \quad (8)$$

$$\frac{\partial(\alpha_c \rho_c \varepsilon_c)}{\partial t} + \nabla.(\alpha_c \rho_c \mathbf{v}_c \varepsilon_c) = \nabla\left[\alpha_c\left(\mu_c + \frac{\mu_{tc}}{\sigma_\varepsilon}\right)(\nabla \varepsilon_c)\right] + \alpha_c \varepsilon_c / k_c (C_{1\varepsilon} G_c - C_{2\varepsilon} \rho_c \varepsilon_c) \quad (9)$$

where k is the turbulent kinetic energy, ε is the turbulence dissipation rate, μ is the molecular dynamic viscosity, μ_t is the turbulent dynamic viscosity and

$$G_c = \mu_{tc}[\nabla \mathbf{v}_c + (\nabla \mathbf{v}_c)^T] : \nabla \mathbf{v}_c \quad (10)$$

With de constants set in $C\mu = 0.09$, $\sigma_k = 1$, $\sigma_\varepsilon = 1.3$, $C_{1\varepsilon} = 1.44$ and $C_{2\varepsilon} = 1.92$.

Turbulence viscosity in the dispersed phase was calculated as

$$\mu_{td} = \left(\frac{\rho_d}{\rho_c}\right)\mu_{tc}/\sigma \quad (11)$$

where $\sigma = 1$.

According to Versteeg and Malalasekera (2007), the flow away from the walls is dominated by inertial effects and in thin layers close to the wall, the viscous effects predominate. Near the wall, the average velocity depends on the distance y from the wall, the shear stress, the specific mass and the viscosity of the fluid.

The logarithmic relation for the near wall velocity is given by:

$$u^+ = \frac{U_t}{u_\tau} = \frac{1}{k}\ln(y^+) + C \quad (12)$$

where:

$$y^+ = \frac{\rho \Delta y u_\tau}{\mu} \quad (13)$$

$$u_\tau = \left(\frac{\tau_\omega}{\rho}\right)^{1/2} \quad (14)$$

u^+ is the near wall velocity, u_τ is the friction velocity, U_t is the known velocity tangent to the wall at a distance of Δy from the wall, y^+ is the dimensionless distance from the wall, τ_ω is the wall shear stress, k is the von Karman constant and C is a log-layer constant depending on wall roughness (Launder, 1974).

For the k-ε model, the reference value for y^+ according to Ansys CFX (2012) is $20 < y^+ < 100$.

The boundary conditions were no-slip condition for liquid and free-slip condition for gas phase on walls. Zero velocity for liquid and 0.25 m/s for gas phase were used. The degassing condition was used on top surface. The time step was 0.005 s.

3. RESULTS

The main mesh used in this study is shown in Fig. 2a, and the cross-section details in Fig. 2b. There were obtained 42,266 nodes and 20,004 elements, these values refer to a coarse mesh in accordance with the reference article. The mesh has about 20% less elements than obtained by Šimčík *et al.* (2011). About the numerical grid, has been used a symmetry plane dividing the reactor in half in the longitudinal plane as shown in Fig. 3 Two types of mesh were applied in the computational domain, one structured in downcomer, and one unstructured in the remainder of the geometry, Šimčík *et al.* (2011) used 48,100 elements.

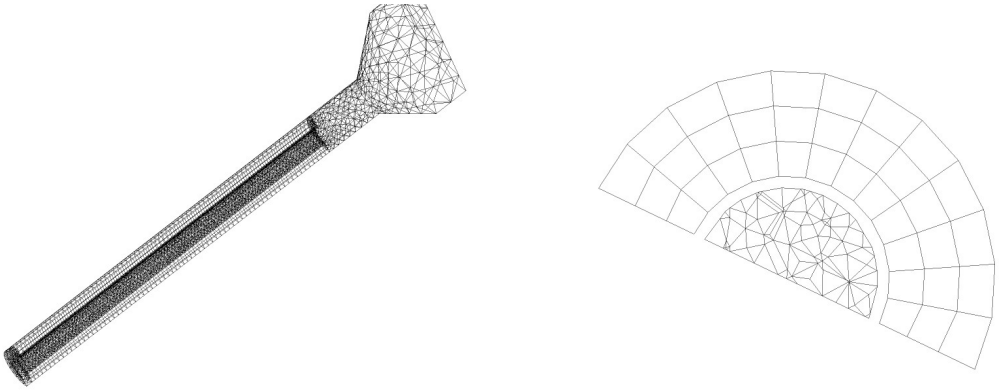

Figure 2. (a) Coarse mesh (left side). (b) Cross-section details (right side).

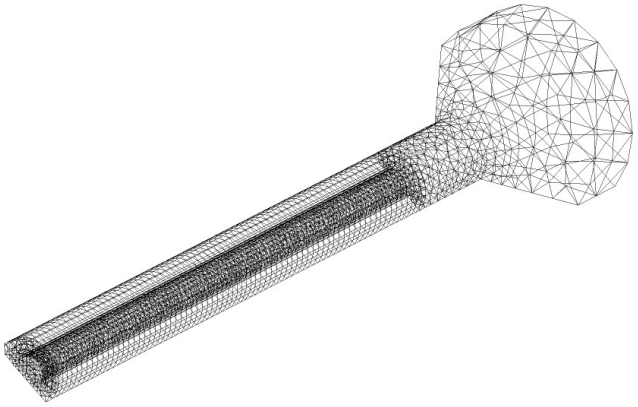

Figure 3. Plane of symmetry.

The parameters verified were the same ones used by Šimčík *et al.* (2011) and later by Xu *et al*. (2015), liquid interstitial velocity in riser, liquid interstitial velocity in downcomer, gas holdup in riser and downcomer. The results are consistent with those published by those authors and are shown in Figs. 4 and 5. There is discrepancy in the simulation results with the highest gas surface velocity, in all parameters except the gas holdup in the downcomer.

However, for the last parameter the simulators presented results with significant differences of the experimental data. The reason of the discrepancy between simulation and experiment is then probably due to the experimental method used to obtain estimates of gas holdups. Holdup estimates measured with U-tube manometers can be negatively influenced by pressure drop due to flow, according to Šimčík *et al.* (2011). Xu *et al*. (2015) propose a different approach in the shape of the bubbles and their interaction with the continuous phase obtaining a result closer to the experimental one, however, the results of the velocities were less accurate.

Figure 6 shows the results for gas holdup obtained with the gas flow rate of 9.1 l/min for both works and it can be observed that there are no significant differences.

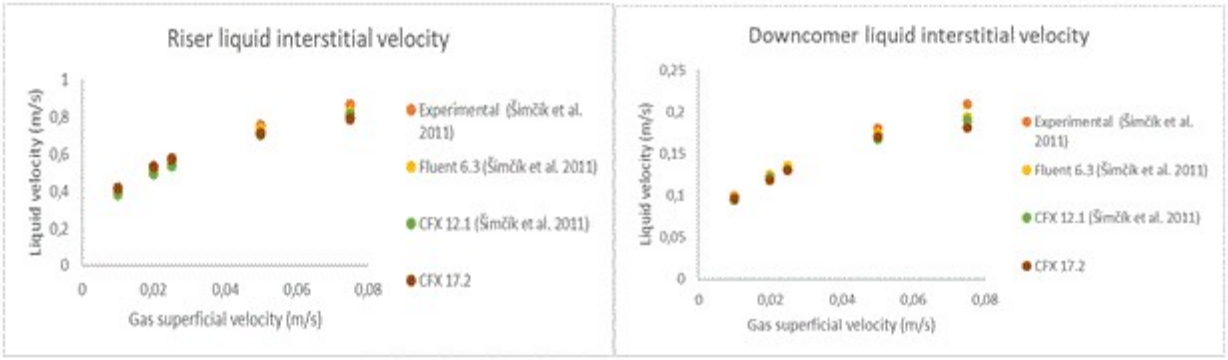

Figure 4. Riser and Downcomer liquid interstitial velocity.

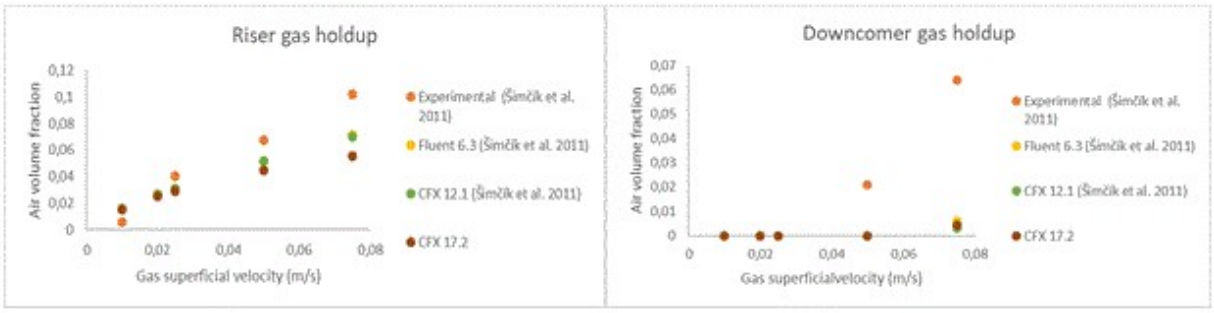

Figure 5. Riser and Downcomer gas holdup.

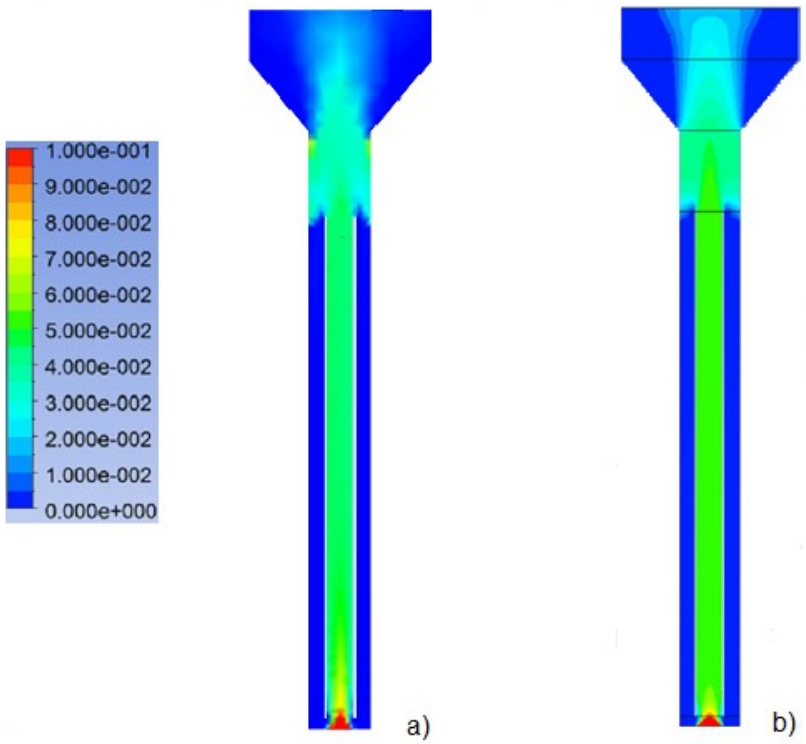

Figure 6. Gas holdup fields for gas flow rates of 9.1 l/min: a) present work, b) Šimčík *et al*. (2011).

New simulations were made for the 0.025 m/s superficial gas velocity with three different meshes for independence test. A factor of 8 was used for each mesh refining.

The coarse mesh had 51,379 elements and 212,055 nodes, with predominance of hexahedral elements. The average quality of the elements was 0.82521 with a standard deviation of 0.22556. Two cross-sections are showed in Fig. 7, the first one with 1 m high and the second at the top. In Fig. 8 is shown a histogram with the elements quality and its distribution.

Finally, the mean y^+ was 85.5 which is in accordance whit the reference values, but the maximum value was 307.7. Its indicate that the mesh isn't fine enough. Figure 9a shows a profile of y^+ in the whole domain.

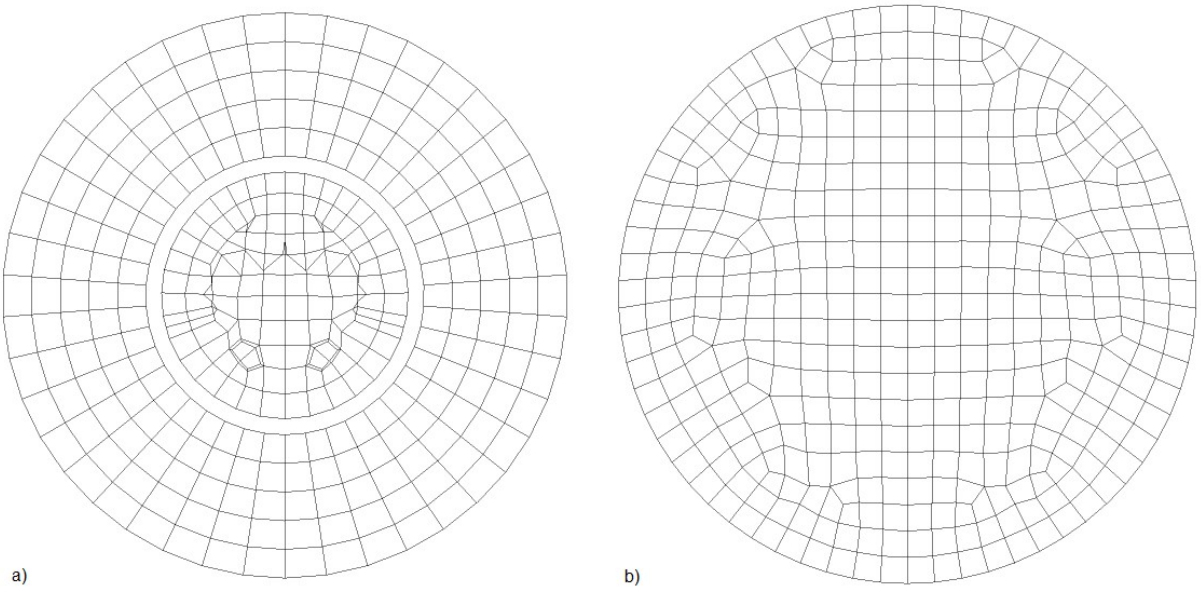

Figure 7. Coarse mesh. A) Cross-section with 1 m high showing the mesh for the riser (inner) and downcomer (external). B) Cross-section in the top.

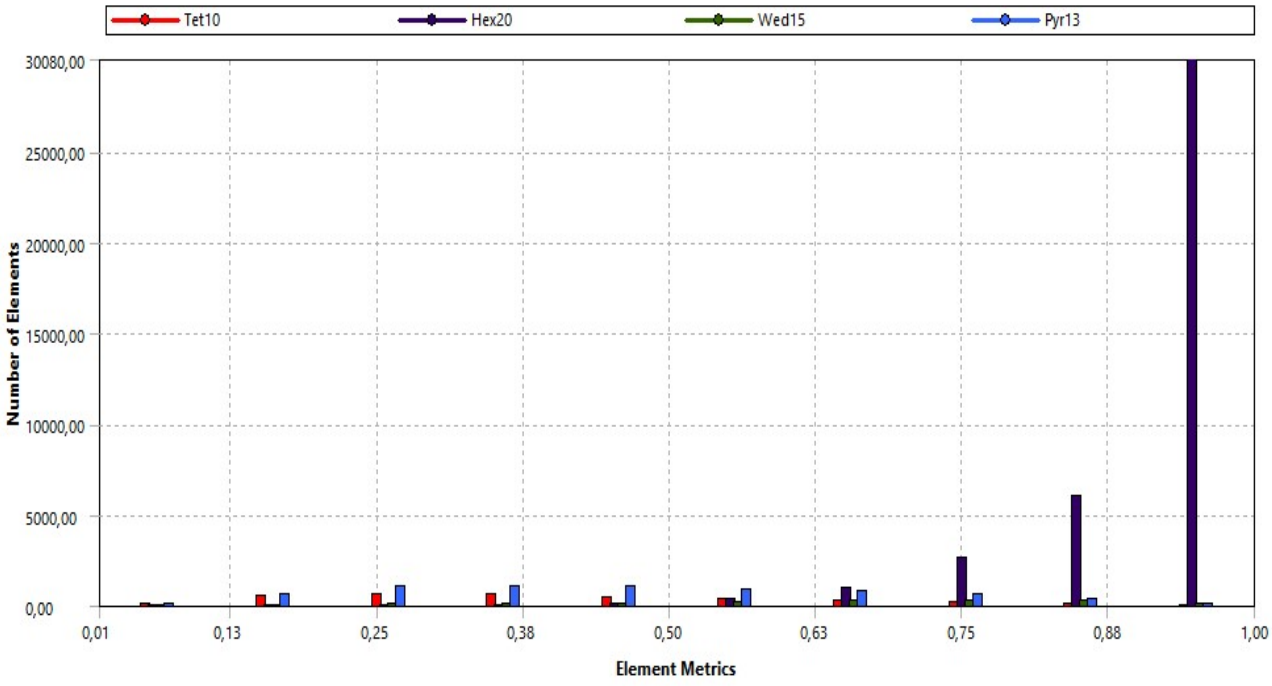

Figure 8. Quality of the elements in the coarse mesh.

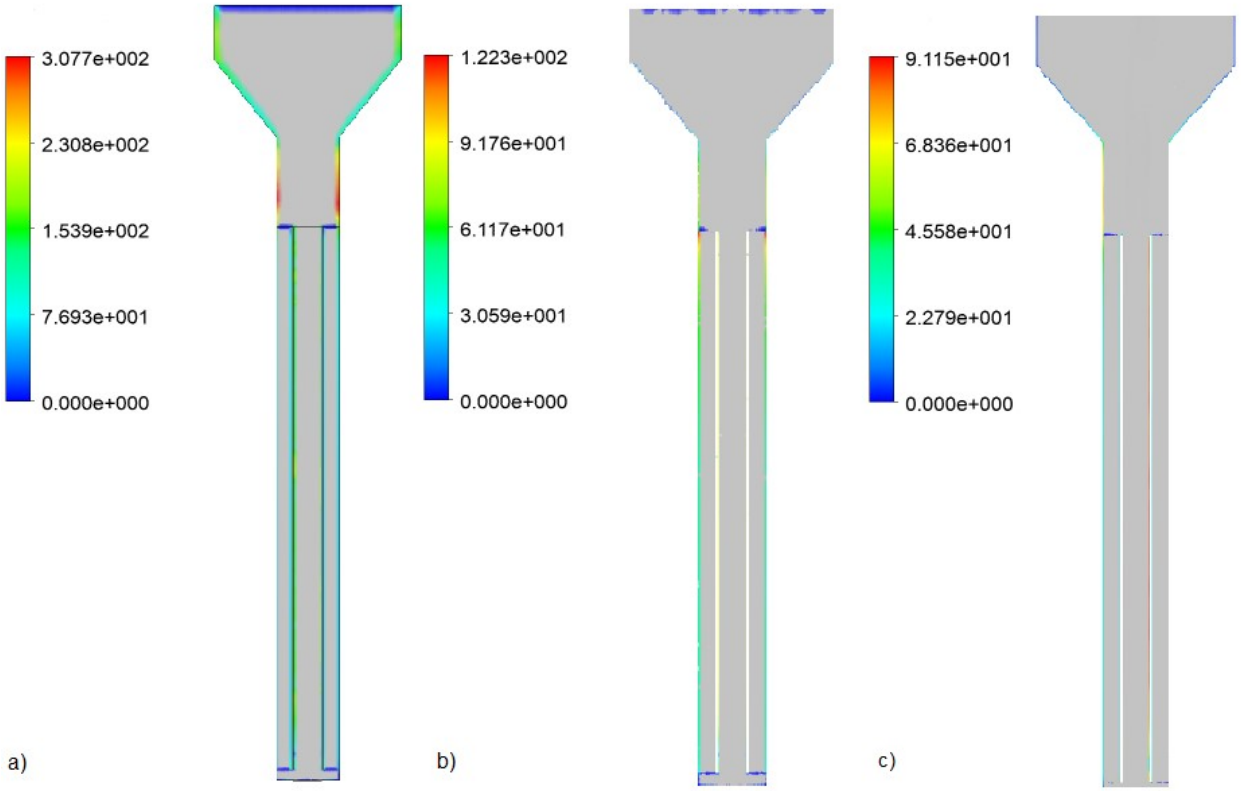

Figure 9. A y^+ profile. A) Coarse mesh. B) Intermediate mesh. C) Refined mesh.

The intermediate mesh presented 382,035 elements and 661,166 nodes being predominantly constituted by tetrahedral elements. Moreover, it presented an average element quality of 0.82802 and a standard deviation of 0.10974. As same as for the coarse mesh Fig. 10 shows two details of the cross-sections and Fig. 11 a histogram on the quality of the elements and its distribution.

The mean y^+ value was 40.15 and the maximum of 122.3, a profile of the y^+ for the intermediate mesh is shown in Fig. 9b.

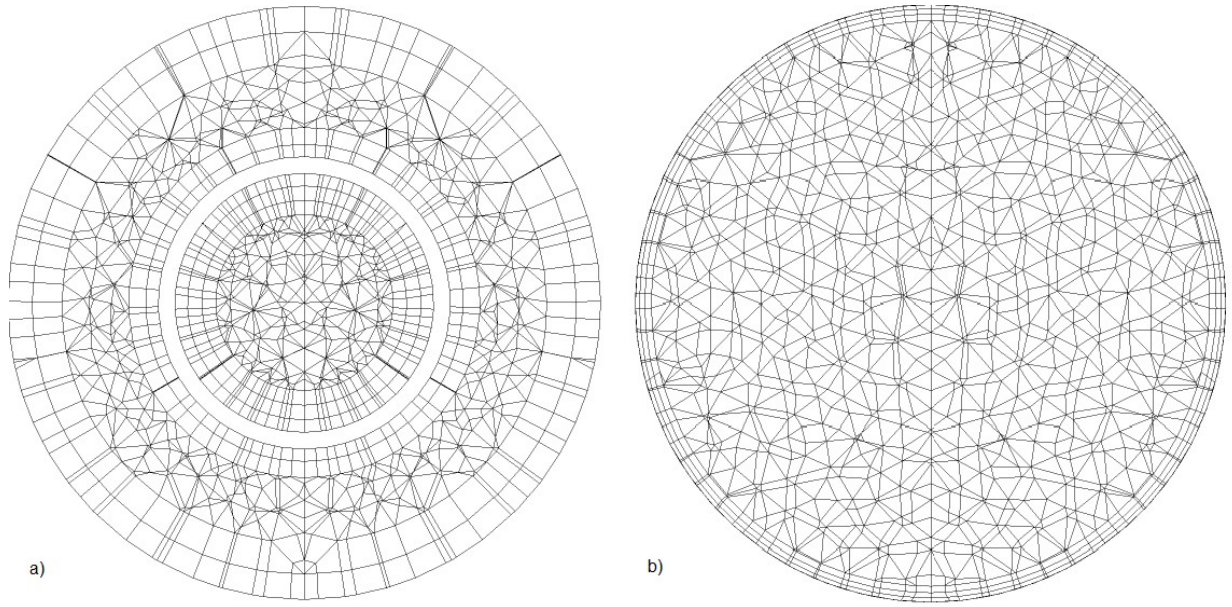

Figure 10. Intermediate mesh. A) Cross-section with 1 m high showing the mesh for the riser (inner) and downcomer (external). B) Cross-section in the top.

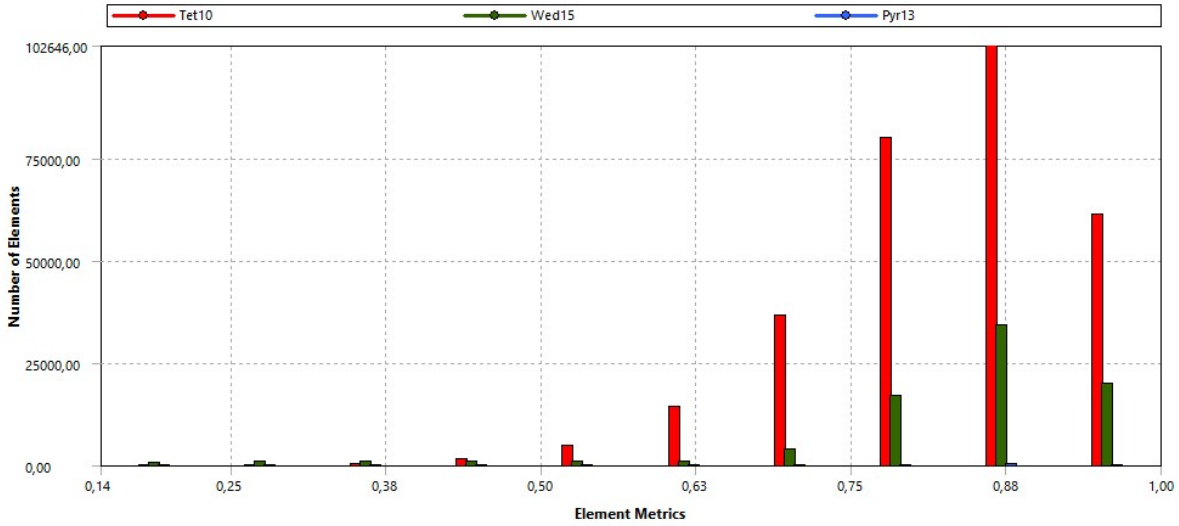

Figure 11. Quality of the elements for the intermediate mesh.

The refined mesh contained 2,960,753 elements and 4,586,582 nodes, basically composed by elements of tetrahedral form. The average mesh quality was 0.8503 whit a standard deviation of 0.0948, its distribution is shown in figure 12. The mesh details are in figure 13.

The maximum value for the y^+ was 91.15 and the average was 26.38 which is in full compliance whit the reference value. A profile of the y^+ is shown in Fig. 9c.

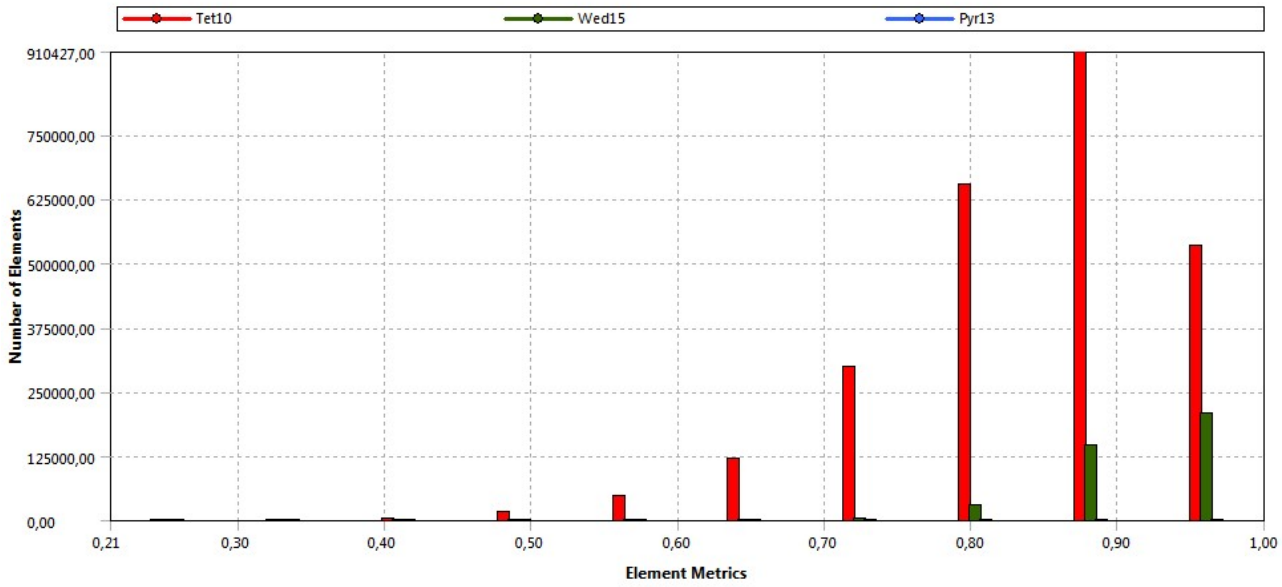

Figure 12. Quality of the elements for the refined mesh.

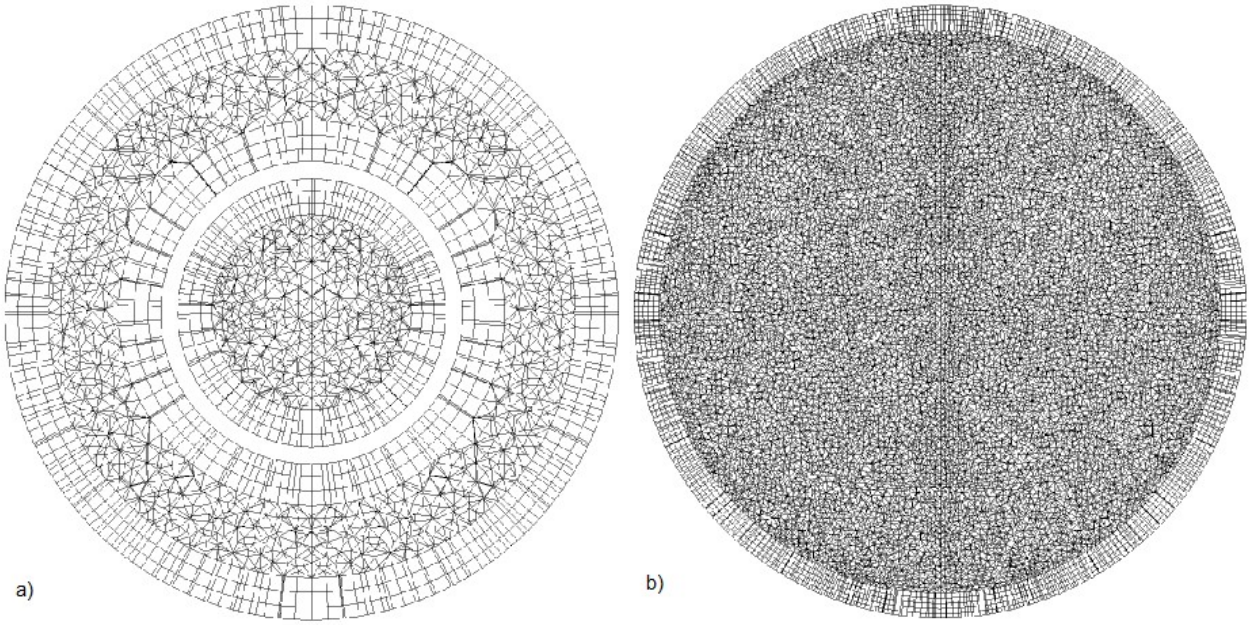

Figure 13. Cross-section details of refined mesh. a) 1 m high. b) Top of reactor.

The results of the new simulations are shown in Fig. 14. For the gas holdup at the downcomer, the results were null, even the experimental ones. Therefore, were omitted from figure. Except for the liquid velocity in the riser the results are in good agreement whit the experimental ones and the results improve as the refining of the mesh increases.

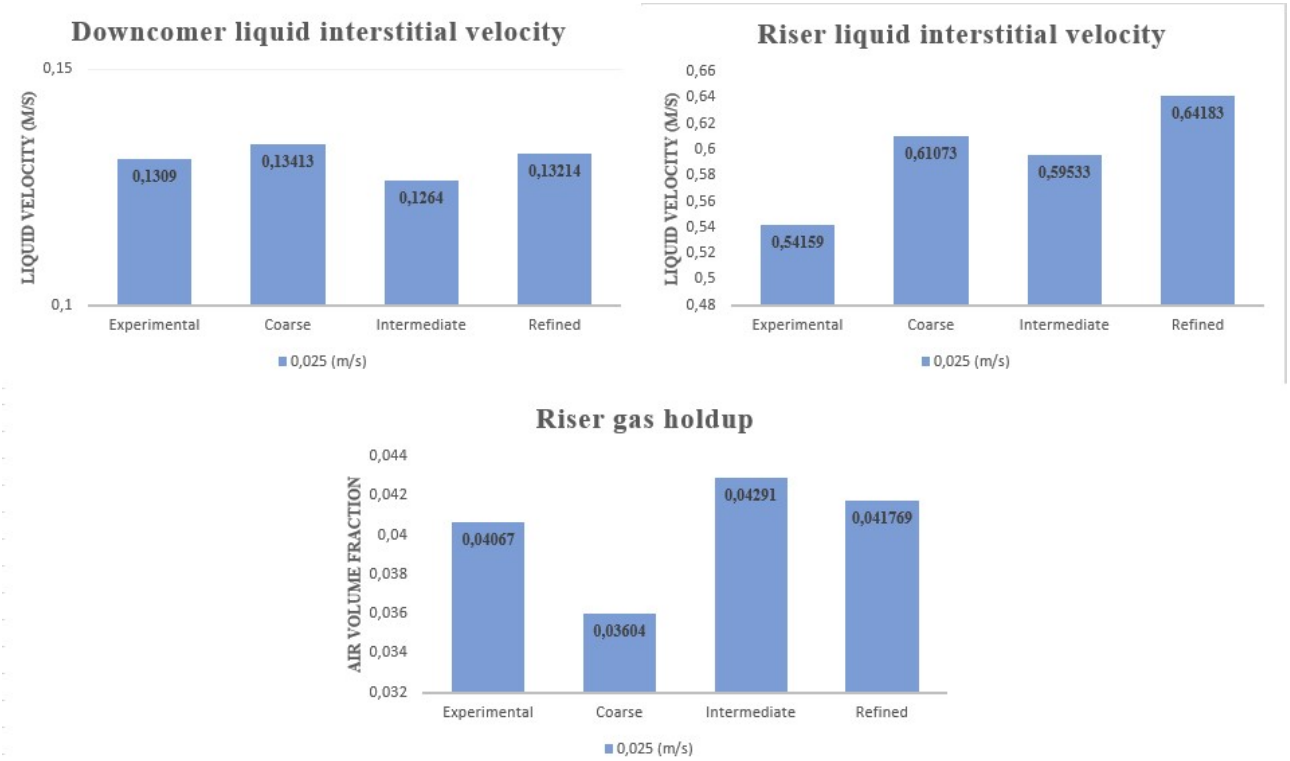

Figure 14: Comparison between coarse, medium meshes and experimental values.

4. CONCLUSIONS

Even with all the information contained in the authors' papers, some important ones are omitted. In the case under study, the values of the volumetric fractions of air at the entrance were not indicate and variation of them interferes effectively in the results. Therefore, the variations found in the results values may be due to different values used for this parameter.

With the simulations in the mesh test, we could observe more details in the flow when executed in refined meshes, however the computational time is much higher than in coarse mesh. If the purpose is to find a global behavior of the fluids, it is not worth the time spent in refined meshes, since the results are quite similar.

Even with about 20% less elements in the mesh, the results were verified demonstrating once again that they are independent of the mesh at these levels, keeping in mind that Šimčík *et al.* (2011) had no significant change in his results with a refined mesh. There is coherence between the values found numerically and the experimental ones, except in the case of the gas holdup in the downcomer section for the highest flow. However, as mentioned earlier, this may be due to failures in the experimental procedure or indeed in mathematical models.

Assuming that the models are adequate and describe the dynamics of the fluids in the reactor. Further studies will be possible in its geometry, in its dimensions proposing a scale-up and in other fronts as thermal and mass transfers inside the airlift.

5. ACKNOWLEDGEMENTS

The authors would like to acknowledge Pontifical Catholic University of Paraná and the Coordination for the Improvement of Higher Education Personnel (CAPES) for the scholarship provided to the first author, as well as, the last author would like to thanks National Council of Scientific and Technologic Development of Brazil - CNPq (grants: 405101/2016/3, and 303906/2015-4-PQ).

6. REFERENCES

AL-MASHHADANI, M. K. H.; WILKINSON, S. J.; ZIMMERMAN, W. B. Airlift Bioreactor for Biological Applications with Microbubble Mediated Transport Processes. Chemical Engineering Science, v. 137, p. 243–253, 2015. Elsevier. <http://dx.doi.org/10.1016/j.ces.2015.06.032>. .

BELLO, R.A.; ROBINSON, C. W.; MOO-YOUNG, M. Gas holdup and overal volumetric oxygen transfer coefficient in airlift contactors. Biotechnology and Bioengineering, v. 27, n. 3, p. 369-381, 1985

CHEN, N. Y. The Design of Airlift Fermenters for Use in Biotechnology. Biotechnology and Genetic Engineering Reviews, v. 8, n. 1, p. 379–396, 1990. <http://www.tandfonline.com/doi/abs/10.1080/02648725.1990.10647875>. .

CHISTI, M. Y. Airlift bioreactors. 1 ed., New York: Elsevier Ltd, 1989.

LAUNDER, B. E.; SPALDING, D. B. The Numerical Computation of Turbulent Flows. Computer Methods in Applied Mechanics and Engineering, v. 3, n. 2, p. 269–289, 1974.

MERCHUCK, J. C. *et al*. Concentric-tube airlift reactors: Effects of geometrical design on performance. AIChE Journal, v. 40, n. 7, p. 1105-1117, 1994.

MERCHUK, J. C.; GLUZ, M. Bioreactors, Air-lift Reactors. Encyclopedia of Bioprocess Technology, p. 320–324, 2002.

SIEGEL, M. H.; MERCHUCK, J. C. Mass transfer in a rectangular airlift reactor. Effects of geometry and gas recirculation. Biotecnology and Bioengineering, v. 32, n. 9, p. 1128-1137, 1988

ŠIMČÍK, M.; MOTA, A.; RUZICKA, M. C.; VICENTE, A.; TEIXEIRA, J. CFD Simulation and Experimental Measurement of Gas Holdup and Liquid Interstitial Velocity in Internal Loop Airlift Reactor. Chemical Engineering Science, v. 66, n. 14, p. 3268–3279, 2011.

User's Manual Version 14.5, 2012. Copyright 1996-2012 ANSYS® Europe Ltd.

VERSTEEG, H.K., MALALASEKERA, W. An Introduction to Computational Fluid Dynamics: The Finite Volume Method. England. Pearson Education Limited, 403p., 2007.

XU, T.; JIANG, X.; YANG, N.; ZHU, J. CFD Simulation of Internal-loop Airlift Reactor Using EMMS Drag Model. Particuology, v. 19, p. 124–132, 2015. Chinese Society of Particuology.<http://dx.doi.org/10.1016/j.partic.2014.04.016>. .

7. RESPONSIBILITY NOTICE

The authors are the only responsible for the printed material included in this paper.